Supplemental Data

Table S1, related to Figure 1.

Parameter	CHZ868
Physicochemical properties	
MW	423
logP	3.9
PSA	83
pK_a	5.5/4.3
Intrinsic solubility (μM)	6
log PAMPA permeability ($cm \cdot s^{-1}$)	-3.6
Liver microsomal stability	
Hepatic extraction mouse/rat/human (%)	69/64/35
CYP3A4/2C9/2D6 (μM)	>20/17.4/18.3
Plasma protein binding mouse/human (%)	98/98
Pharmacokinetic properties in mice (n=3)	
Dose IV/PO ($mg \cdot kg^{-1}$)	2.5/10
CL ($mL \cdot min^{-1} \cdot kg^{-1}$)	38
V_{ss} ($L \cdot kg^{-1}$)	2.7
$t_{1/2\ term.}$ (hr)	1.0
AUC IV d.n. (nM·hr)	1038
AUC PO d.n. (nM·hr)	521
C_{max} d.n. (nM)	201
T_{max} (hr)	0.5
BAV (%)	50

Dose IV 2.5 $mg \cdot kg^{-1}$ (NMP:plasma 10:90).

Dose PO 10 mg·kg-1 (Tween80:CMC05 0.5:99.5).

Parameter dose-normalized (d.n.) to 1 $mg \cdot kg^{-1}$.

A

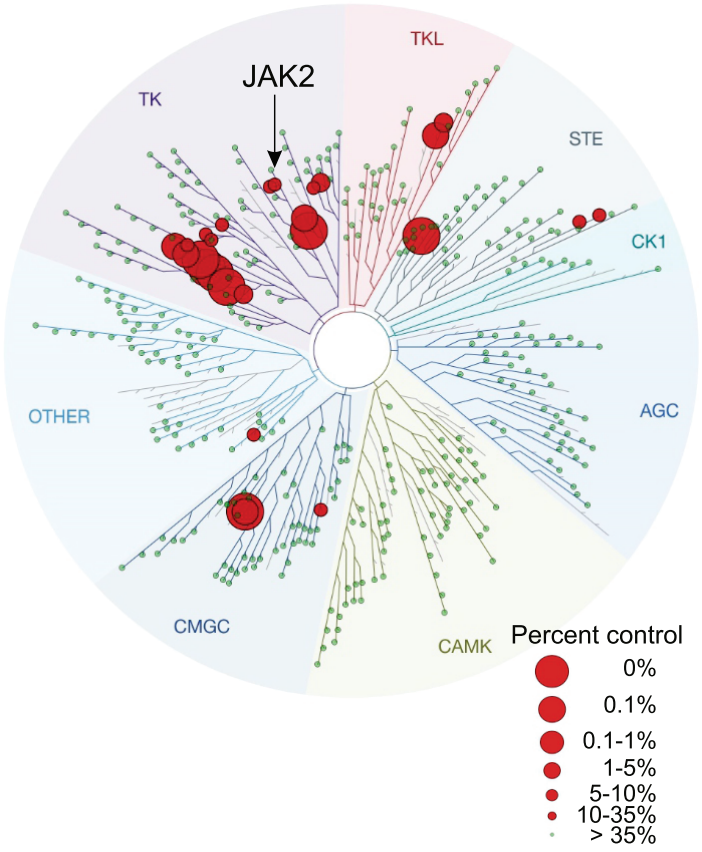

B

KINOMEscan (percent control)		Cellular Assay (IC_{50}, nM)	
ABL1-nonphosph.	10	Ba/F3 BCR-ABL	6266
ABL2	33	NA	
BRAF	4.3	Ba/F3 BRAF V600E	825
BRK	25	NA	
CRAF	5.3	NA	
CDC2L1	2.4	NA	
CDC2L2	0.8	NA	
CSF1R	0.9	NA	
DDR1	0.5	NA	
DDR2	2.2	NA	
GCN2	21	NA	
INSRR	9.4	NA	
JAK2	16	Ba/F3 JAK2 V617F	51
KIT	0.8	Ba/F3 TEL-KIT	16
MAP3K2	12	NA	
MAP3K3	25	NA	
PDGFRA	8.7	Ba/F3 TEL-PDGFRA	23
PDGFRB	0.15	Ba/F3 TEL-PDGFRB	4
RET	24	Ba/F3 TEL-RET	8842
ROS1	33	Ba/F3 TEL-ROS	40
SRPK1	34	NA	
TAOK2	0.3	NA	
TYK2	26	NA	
VEGFR1	1.6	Ba/F3 TEL-VEGFR1	2
VEGFR2	1.4	Ba/F3 TEL-VEGFR2	11
VEGFR3	0.95	NA	

C

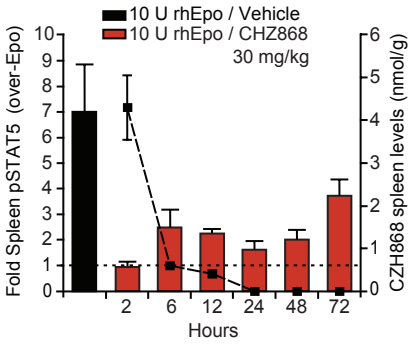

D

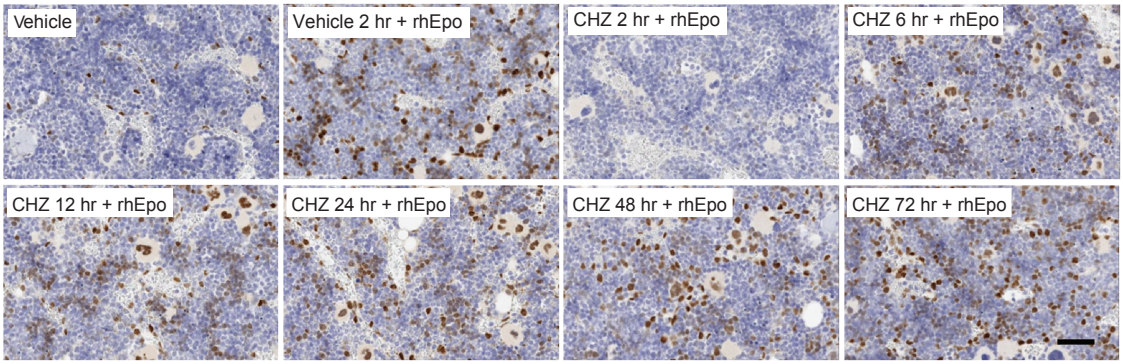

E

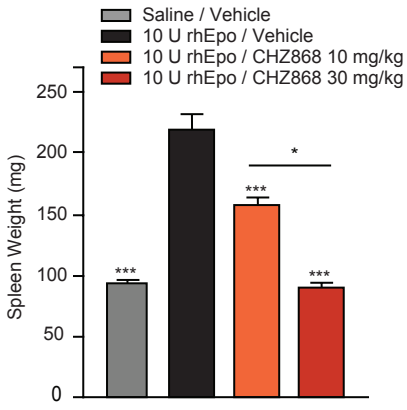

F

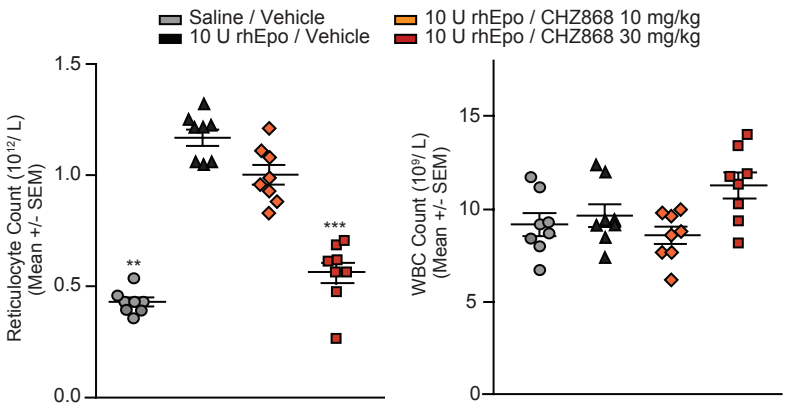

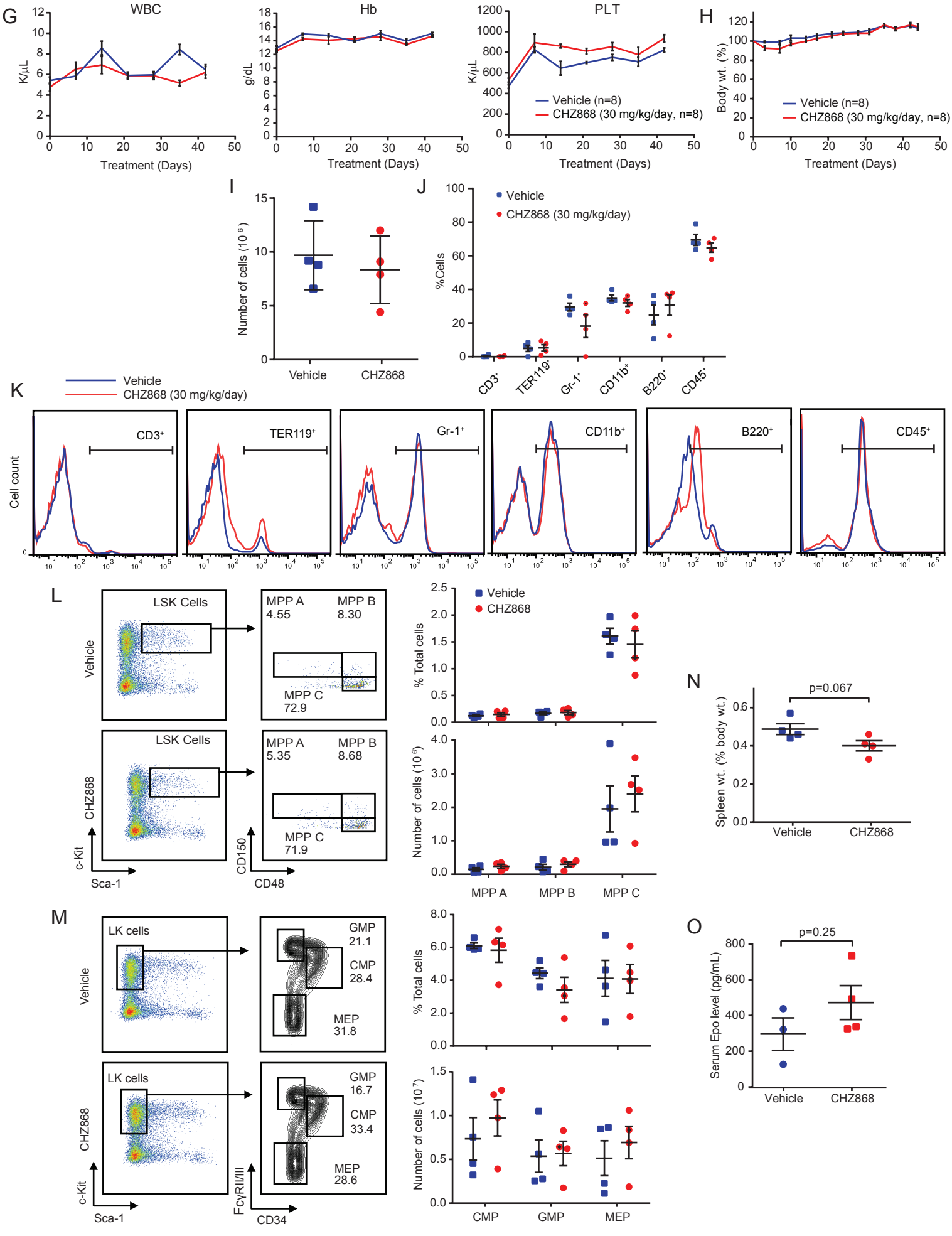
G
WBC
K/μL
Hb
g/dL
PLT
K/μL
Treatment (Days)
Vehicle (n=8)
CHZ868 (30 mg/kg/day, n=8)
H
Body wt. (%)
I
Number of cells (10 6)
Vehicle
CHZ868
J
Vehicle
CHZ868 (30 mg/kg/day)
%Cells
CD3+
TER119+
Gr-1+
CD11b+
B220+
CD45+
K
Cell count
L
LSK Cells
MPP A
4.55
MPP B
8.30
MPP C
72.9
5.35
8.68
71.9
CHZ868
c-Kit
Sca-1
CD150
CD48
% Total cells
Number of cells (10 6)
MPP A
MPP B
MPP C
N
p=0.067
Spleen wt. (% body wt.)
M
LK cells
GMP
21.1
16.7
CMP
28.4
33.4
MEP
31.8
28.6
FcγRII/III
CD34
Number of cells (10 7)
CMP
GMP
MEP
O
p=0.25
Serum Epo level (pg/mL)

Figure S1, related to Figure 1. CHZ868 in vitro kinase, in vitro cellular, and in vivo activity. **(A)** CHZ868 was screened against a panel of 403 recombinant kinases at a test concentration of 100 nM. The TREEspot™ visualization depicts kinase phylogeny captured on the solid support (atypical, lipid, and pathogen kinases not shown), with kinases interacting with CHZ868 represented as red circles. The larger the red circle diameter, the higher the CHZ868 binding affinity and the less kinase captured on the solid support, respectively. **(B)** Left column: Binding interactions of the 26 hits reported as ≤35% percent of control, where lower numbers indicate stronger hits. Right column: IC_{50} values of hits determined in corresponding Ba/F3 cell-based proliferation assays over 48 hr. NA: Corresponding Ba/F3 cell-based assay not available. **(C)** BALB/c mice (female, n=3/group) received CHZ868 30 mg/kg or vehicle by oral gavage. Sampling was performed on individual cohorts at indicated timepoints. 3 hr prior to each sampling timepoint, mice received 10 U rhEpo or saline subcutaneously. Spleen samples were extracted for detection of levels of pSTAT5 by Meso Scale Discovery technology (fold induction over saline (-rhEpo) depicted by dotted line). Closed squares and dashed line represent CHZ868 levels determined in spleen extracts at the respective time points after dosing. Error bars indicate SEM. **(D)** Representative immunohistochemistry (IHC) for pSTAT5 in sternal bone marrow. Scale bar, 50 μm. **(E)** BALB/c mice (female, n=8/group) received vehicle or CHZ868 at 10 mg/kg or 30 mg/kg for 4 consecutive days. Mice also received 10 U rhEpo daily or saline control. Spleen weight was assessed on day 5, 24 hr after last treatment. *p<0.05 and ***p<0.001 versus rhEpo/vehicle group by one-way ANOVA, followed by Dunnett's test and Tukey's test on log-transformed values. **(F)** Reticulocyte count and white blood cell count post-therapy are shown. Blood samples were assessed using the Sysmex blood analyzer. Plots depict the individual data points in the different treatment groups. Statistical analysis: One-way ANOVA, followed by Dunnett's test or Tukey's test for multiple comparisons (on square root-transformed values for reticulocyte count). **p<0.01, ***p<0.001 versus rhEpo/vehicle group. 6-week-old FVB/NJ x C57B6/J F1 hybrid mice were treated with vehicle (n=8) or CHZ868 30 mg/kg/day (n=8) for 6 weeks**. (G)** Complete blood counts were performed on peripheral blood every 7 days. Total white blood cell count (WBC), hemoglobin (Hb) and platelet counts (PLT) are shown. **(H)** Body weight relative to day 0 of the mice treated with vehicle or CHZ868. **(I)** Number of cells harvested from 1 femur per mouse after 6 weeks of vehicle or CHZ868 treatment. **(J)** Percentage distribution of lineage positive cells in bone marrow harvested from 1 femur of mice after 6 weeks of vehicle or CHZ868 treatment and analyzed by flow cytometry. **(K)** Representative flow plots of the distribution of indicated cell surface marker in the vehicle or CHZ868 group. **(L)** In order to test the possibility that JAK2 inhibition by CHZ868 affects hematopoietic progenitor cells, we examined $Lin^{-}c\text{-}Kit^{+}Sca\text{-}1^{+}$ (LSK) hematopoietic stem cells and $Lin^{-}c\text{-}Kit^{+}Sca\text{-}1^{-}$ (LK) myeloid progenitor populations (Kiel et al., 2005). Mice treated for 6 weeks with either CHZ868 or vehicle had similar proportions of LSK cells as well as LSK subpopulations. MPP A ($CD34^{-}CD150^{+}$) contain long-term hematopoietic stem cells while MPP B ($CD34^{+}CD150^{-}$) and MPP C ($CD34^{+}CD150^{-}$) contain short-term hematopoietic stem cells. Percent of total cells indicates flow cytometry results after Lin^{+} were partially depleted using Sheep anti-rat IgG conjugated magnetic beads (see Supplemental Methods). **(M)** Mice treated with CHZ868 or vehicle for 6 weeks had similar frequencies of LK populations. We examined $F\gamma R^{hi}CD34^{+}$ common myeloid progenitors (CMPs), $F\gamma R^{lo}CD34^{+}$ granulocyte/macrophage lineage-restricted progenitors (GMPs) and $F\gamma R^{lo}CD34^{-}$ megakaryote/erythrocyte lineage-restricted progenitors (MEPs). **(N)** Spleen weight as a percentage of body weight for mice after 6 weeks of either vehicle or CHZ868 treatment. **(O)** Erythropoietin levels in the serum after 6 weeks of vehicle or CHZ868 treatment. In all panels of this figure, error bars indicate SEM.

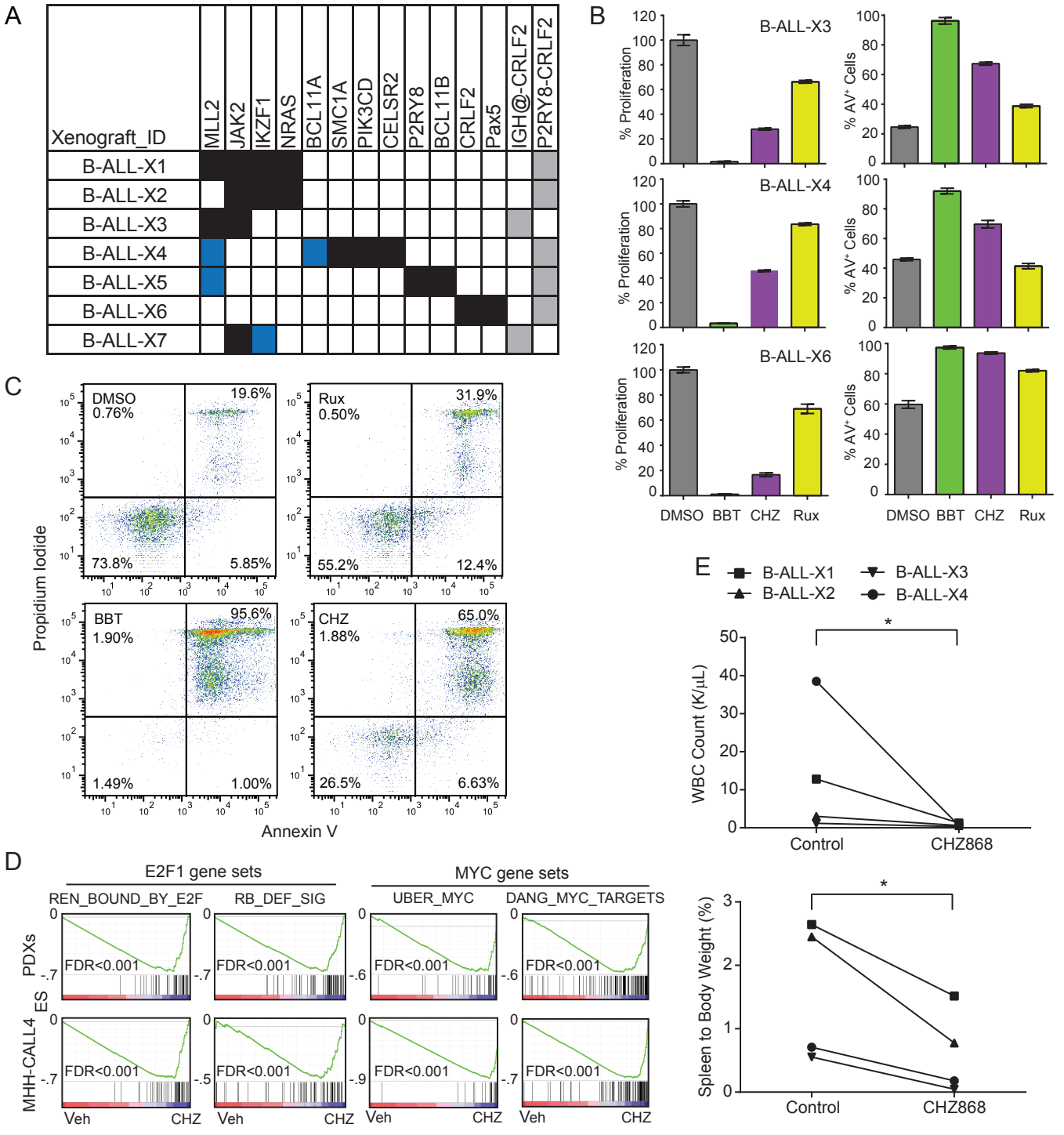

Figure S2, related to Figure 3. CHZ868 inhibits B-ALL proliferation in vitro and in vivo.
(A) Genomic characterization of the *CRLF2*-rearranged PDX models was performed through deep sequencing of >200 genes recurrently mutated in hematologic malignancies (Odejide et al. Blood 2014). Blue boxes indicate the presence of insertion/deletions (INDELs) in a gene and black boxes indicate single-nucleotide variants (SNVs). Specific alterations are listed in Table S2. *CRLF2* rearrangements were determined by RT-PCR for P2RY8-CRLF2 and FISH for IGH@-CRLF2. B-ALL-X1 and B-ALL-X2 are derived from the same patient and differ based on the presence or absence of an *MLL2* mutation. **(B)** *CRLF2*-rearranged PDXs were treated for 48 hours ex vivo with vehicle or 1 μM BBT594 (BBT), CHZ868 (CHZ), or Ruxolitinib (Rux). Proliferation was measured relative to vehicle control using CellTiter Glo. Percentage annexin V (AV^+) positive cells was measured by flow cytometry in the same cells. Error bars represent SEM. **(C)** Representative flow plots of B-ALL-X3 PDX cells treated as in **(B)** and analyzed for Annexin V and Propidium Iodide staining by flow cytometry. **(D)** Gene set enrichment analysis plots of previously defined functional gene sets of either MYC or E2F1 are highly enriched among the genes downregulated by CHZ868 treatment in both PDXs and MHH-CALL4 cells. **(E)** Spleen weight as a percentage of total body weight and peripheral blood WBC count of NSG mice xenografted with the indicated B-ALL PDXs and treated for 6 days with 30 mg/kg/day CHZ868 or untreated control beginning at the time of engraftment (>2% peripheral blood hCD45+ cells). *p<0.05 by two-sided t-test.

Table S2, related to Figure 3.

Xenograft ID	Gene	Chr	Mutation/Effect	Amino acid change	DNA Change	Mutant allele fraction	COSMIC
B-ALL-X1	NRAS	1	Missense	p.G12D	g.115258747G>A	0.496063	Yes
B-ALL-X1	MLL2	12	Nonsense	p.R2645*	g.49433620C>T	0.490085	No
B-ALL-X1	IKZF1	7	Nonsense	p.S41*	g.50367315C>A	0.511254	No
B-ALL-X1	JAK2	9	Missense	p.R683G	g.5078360A>G	0.98961	Yes
B-ALL-X2	NRAS	1	Missense	p.G12D	g.115258747G>A	0.479087	Yes
B-ALL-X2	IKZF1	7	Nonsense	p.S41*	g.50367315C>A	0.502041	No
B-ALL-X2	JAK2	9	Missense	p.R683G	g.5078360A>G	0.996633	Yes
B-ALL-X3	MLL2	12	Nonsense	p.R1615*	g.49438647C>T	0.034188	No
B-ALL-X3	MLL2	12	Splice site	p.S59_splice	g.49448536_splice	0.409938	No
B-ALL-X3	JAK2	9	Missense	p.R683S	g.5078362A>T	0.492157	Yes
B-ALL-X4	SMC1A	X	Missense	p.G707E	g.53432020G>A	0.513423	No
B-ALL-X4	CELSR2	1	Missense	p.D1485G	g.109804976A>G	0.044053	No
B-ALL-X4	PIK3CD	1	Missense	p.F1015Y	g.9787013T>A	0.078947	No
B-ALL-X4	MLL2	12	Frame shift	p.G3702fs	g.49427382GC>C	0.5636	No
B-ALL-X4	BCL11A	2	Frame shift	p.K425fs	g.60688774T>TGGGG	0.0502	No
B-ALL-X5	P2RY8	X	Missense	p.V167A	g.1584952T>C	0.056338	No
B-ALL-X5	BCL11B	14	Missense	p.E879K	g.99640538G>A	0.045249	No
B-ALL-X5	MLL2	12	Frame shift	p.T1277fs	g.49443542T>TC	0.2878	No
B-ALL-X6	PAX5	9	Nonsense	p.Y354*	g.36846877C>A	0.98	No
B-ALL-X6	CRLF2	X	Missense	p.F232C	g.1314966T>G	0.468137	Yes
B-ALL-X7	IKZF1	7	Missense	p.G123V	g.50444438G>T	0.564935	No
B-ALL-X7	JAK2	9	Missense	p.F694C	g.5078394T>G	0.037383	No
B-ALL-X7	IKZF1	7	Frame shift	p.C71fs	g.50444283T>TGA	0.0513	No
B-ALL-X7	IKZF1	7	Frame shift	p.M92fs	g.50444345T**G**A>TGG**G**ATC	0.25	No

COSMIC indicates that the alteration was reported in the Catalog of Somatic Mutations database (http://www.sanger.ac.uk/genetics/CGP/cosmic/)

Table S3, related to Figure 3. Provided as an Excel file.

Table S4, related to Figure 3. Provided as an Excel file.

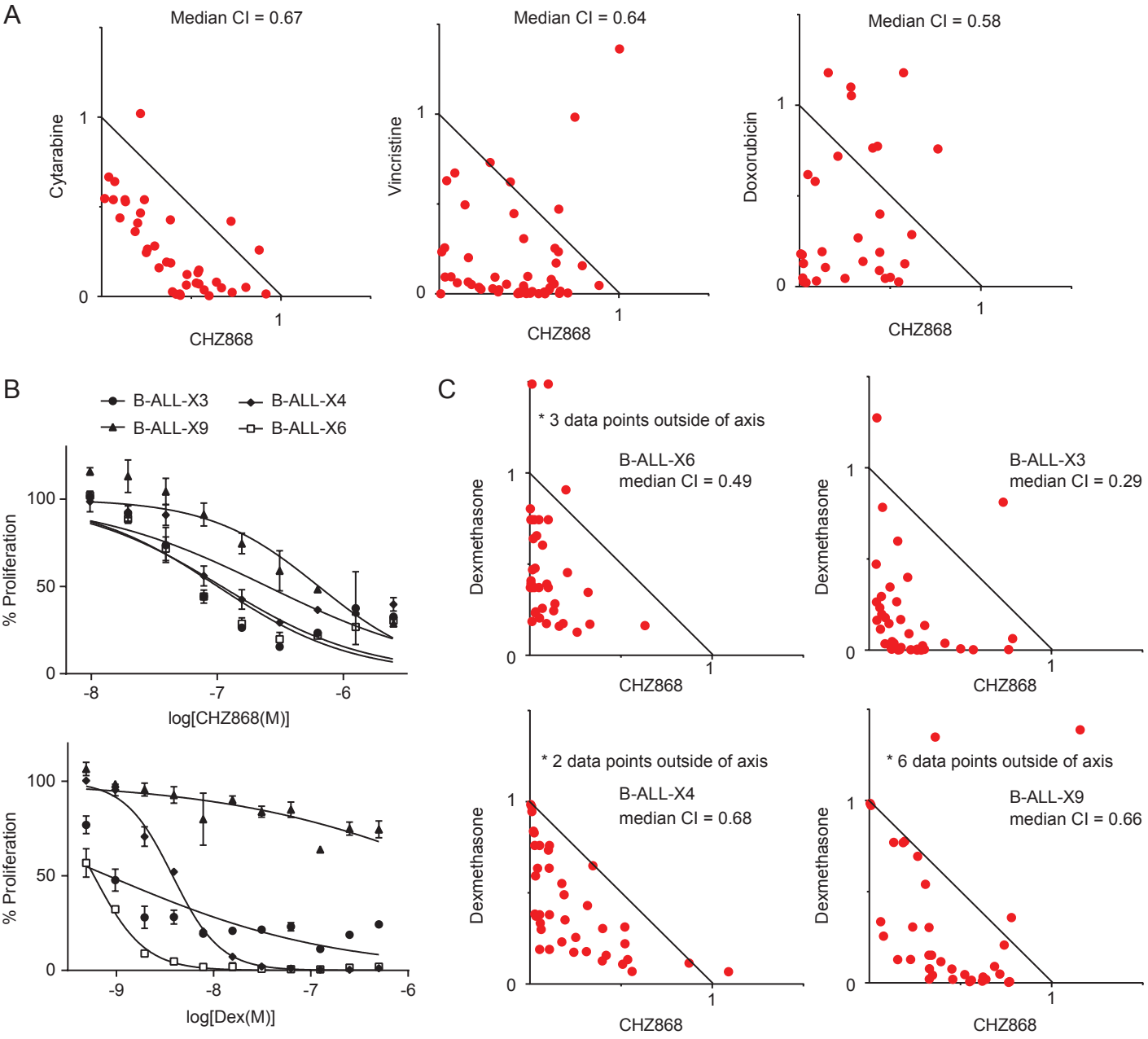

D

GENE SET NAME	SIZE	ES	NES	NOM p val	FDR q val	FWER p val
ALCALA_APOPTOTIC_CELLDEATH	62	-0.5537059	-2.3007147	0	0	0
ALCALA_APOPTOSIS	86	-0.4907143	-2.142819	0	0	0
REACTOME_APOPTOSIS	138	-0.40972316	-1.9537878	0	0	0
KEGG_APOPTOSIS	84	-0.39996326	-1.7736994	0	0	0

Figure S3, related to Figure 4. CHZ868 and conventional chemotherapy combinations in *CRLF2*-rearranged, JAK2-dependent human B-ALL cells and human xenografts.
(A) Isobologram analyses of CHZ868 with the indicated agents at multiple concentrations in MHH-CALL4 cells. Results are from a representative experiment performed in triplicate. CI, combination index. **(B)** Inhibition of cell proliferation by CHZ868 or dexamethasone in PDXs treated ex vivo for 72 hr. Error bars represent SEM. **(C)** Isobologram analyses of CHZ868 and dexamethasone in PDXs treated ex vivo for 72 hr. Median combination index (CI) represents the average of triplicates from a representative experiment. **(D)** Gene set enrichment analysis (GSEA) results for apoptosis gene sets following treatment with dexamethasone plus CHZ868 vs. CHZ868 in MHH-CALL4 cells.

A

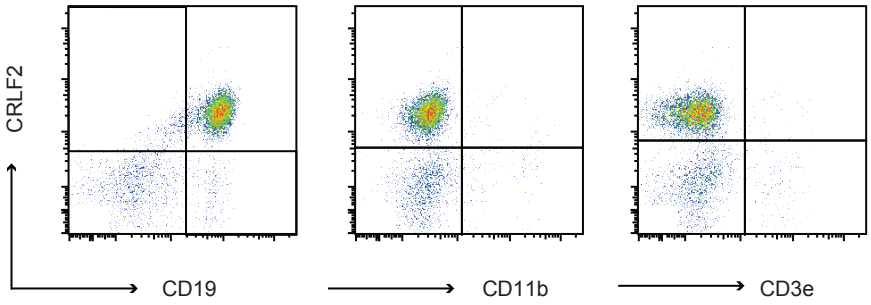

B

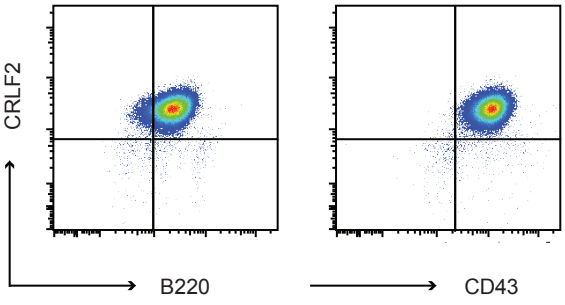

C

Mouse ID	Genotype	Gender	Background	Age at Death
1921	Eμ-*CRLF2* F232C/Ts1Rhr/C*dkn2a* $^{-/-}$	M	FVB/C57B6	263
1946	Eμ-*CRLF2* F232C/Ts1Rhr/C*dkn2a* $^{-/-}$	M	FVB/C57B6	224
1220a	Eμ-*CRLF2*/Eμ-*Jak2* R683G/C*dkn2a* $^{-/-}$	F	FVB	131
1222a	Eμ-*CRLF2*/Eμ-*Jak2* R683G/C*dkn2a* $^{-/-}$	F	FVB	193
2458p	Eμ-*CRLF2*/Eμ-*Jak2* R683G/*Pax5* $^{+/-}$	M	FVB/C57B6	378
2539p	Eμ-*CRLF2*/Eμ-*Jak2* R683G/Ts1Rhr/*Pax5* $^{+/-}$	F	FVB/C57B6	183

D

GENE SET NAME	SIZE	ES	NES	NOM p val	FDR q val	FWER p val
ALCALA_APOPTOSIS	86	-0.6350852	-2.478544	0	0	0
ALCALA_APOPTOTIC_CELLDEATH	62	-0.627835	-2.3560565	0	0	0
REACTOME_APOPTOSIS	138	-0.5274307	-2.2744799	0	0	0
KEGG_APOPTOSIS	84	-0.449774	-1.7623924	0	0	0

Figure S4, related to Figure 5. Establishment of transgenic models of JAK2-dependent B-ALL.
(A) Representative flow cytometry of unselected cells isolated from the spleen of an Eμ-*CRLF2*/Eμ-*Jak2* R683G/*Cdkn2a*$^{-/-}$ mouse (line 1220a) showing expression of a CRLF2^{+}CD11b^{-}CD3e^{-} population. **(B)** Gating on the *CRLF2*-expressing population reveals the cells to be B220^{+}CD43^{+}. **(C)** Established transgenic B-ALLs. All lines express *CRLF2* and cause fatal disease in secondary transplant recipients. **(D)** Gene set enrichment analysis (GSEA) results for apoptosis gene sets following treatment with dexamethasone plus CHZ868 vs. CHZ868 in patient-derived xenografts (PDXs).

Supplemental Experimental Procedures

Inhibitors

For in vitro studies, all compounds were resuspended in DMSO to make 10 mM stock solutions (stored at -20°C) and diluted to appropriate concentrations prior to use. For in vivo studies, CHZ868 was reconstituted in 0.5% methylcellulose / 0.5% Tween-80 and administered at doses of 30 mg/kg/day by oral gavage. Dexamethasone was reconstituted in saline and administered at doses of 1 mg/kg/day by intraperitoneal injection.

Broad CHZ868 kinase selectivity was assessed in competition binding assays, using a panel of 403 recombinant kinases (DiscoveRx KINOMEscan^{TM}) as described (Karaman et al., 2008). CHZ868 was tested at a concentration of 100 nM to be in the range of JAK2-dependent cell-based assay IC_{50} values, and the free-drug exposure at C_{max} achieved in vivo in the mouse models at efficacious doses (30 mg/kg), taking into account the percentage of compound plasma protein binding.

Generation of U2OS cells stably expressing EpoR and STAT5a-eGFP

Human osteosarcoma U2OS cells (ATCC, HTB-96) were cultured in RPMI medium supplemented with 10% of fetal calf serum (FCS), 2 mM L-glutamine and 1 % (v/v) penicillin/streptomycin. U2OS clones expressing EpoR and STAT5a-eGFP proteins were cultured in the aforementioned medium supplemented with 400 µg/mL of Geneticin (G418; 11811-031, Invitrogen) and 100 µg/mL Hygromycin B (10687-010, Invitrogen) to maintain expression of STAT5a-eGFP and EpoR, respectively.

For stable transfection of STAT5a-eGFP, U2OS cells were grown in a 10-cm plate to reach 70% confluency. Before transfection, cells were washed once with PBS followed by addition of 8.5 mL fresh medium without antibiotics. 15 µg of STAT5a-eGFP plasmid (EX-F0979-M03, GeneCopoeia; the STAT5a cDNA sequence contained a non-synonymous mutation which was corrected according to the reference sequence NM_003152 by Solvias, Basel, Switzerland) and 40 µl of lipofectamine 2000 (1 mg/mL; 11668-027, Invitrogen) were individually diluted in 750 µl of OptiMEM (51985-026, Invitrogen) and incubated for 5 min at room temperature. cDNA and lipofectamine solutions were combined, incubated for 20 min at room temperature and added dropwise to the cells. Medium was changed 6 hr post-transfection to avoid cytotoxicity due to lipofectamine. Plasmid transfected and mock-transfected cells were then put under selection with 400 µg/mL G418. Once all mock-transfected cells were dead, freezing stocks were made from the U2OS-STAT5a-eGFP pool.

For stable transfection of EpoR, U2OS cells stably expressing STAT5a-eGFP were grown in a 6-cm dish in 4 mL of medium without antibiotics and incubated at 37°C to reach 95% confluency. 8 µg of pcDNA3.1/Hygro:EpoR plasmid (Invitrogen) and 20 µl of lipofectamine 2000 were separately added to 500 µl of OptiMEM and incubated for 5 min at room temperature. Plasmid and lipofectamine solutions were then mixed and incubated for 20 min at room temperature. Resulting complexes were added drop wise to the cells and incubated for 6 hr at 37°C before changing medium. 1 day post-transfection, 400 µg/mL G148 and 100 µg/mL Hygromycin B were added to the medium to select for STAT5a-eGFP and EpoR expression, respectively. Some cryogenic vials of the pool were prepared as soon as the mock-transfected U2OS-STAT5a-eGFP cells had died in the presence of Hygromycin B.

In order to isolate single U2OS clones that stably express both STAT5a-eGFP and EpoR, five 96-well plates were seeded with transfected U2OS cells diluted to 0.5 cell per well and incubated for 10 days at 37°C. Plates were observed by fluorescence microscopy using the FITC filter to select clones expressing STAT5a-eGFP protein. 19 GFP-positive colonies were amplified stepwise in bigger wells/plates until they reached reasonable cell numbers for further characterization, which involved assessment of erythropoietin-responsiveness of STAT5 phosphorylation (Western blotting), and of STAT5 translocation from cytoplasm to nucleus (microscopy), respectively. These efforts led to the selection of U2OS STAT5a-eGFP-EpoR clone 13 cells for use in the Cellomics JAK2-dependent STAT5 nuclear translocation assay.

Cellomics nuclear translocation assay with U2OS STAT5a-eGFP-EpoR cells

JAK inhibitors were tested in the JAK2-dependent STAT5 nuclear translocation assay as follows: U2OS STAT5a-eGFP-EpoR clone 13 cells were seeded at a cell density of 12,000 cells per well in 96-well Black Packard View-Plates™ (6005182, PerkinElmer Inc) and incubated at 37°C. The following day, medium was removed and 90 µl per well of medium containing either the vehicle DMSO (diluted to 1:2272) or increasing concentrations of inhibitors (inhibitors are 1.1 x concentrated for pretreatment) for 30 min at 37°C. Cells were then stimulated for 1 hr by adding 10 µl per well of 50 U/mL rhEpo (recombinant ultra-pure human erythropoietin; CRE600B, Cell Sciences) to obtain 5 U/mL of rhEpo as the final concentration.

Then, medium was removal and cells were fixed with 100 µl/well of 3.7 % formaldehyde (F-1635, Sigma-Aldrich; diluted in PBS) for 10 min at room temperature. Next, cells were washed twice with 200 µl PBS per well and stained with 100 µl of 10 µg/mL Hoechst 33342 DNA binding dye (H-3570, Molecular Probes; diluted in PBS) per well for 5 min at room temperature in the

dark. After 2 additional washes with PBS, wells were filled with 200 µl PBS per well and either covered with a black lid and stored at 4°C, or analyzed with the Cellomics device immediately.

Two-channel fluorescence microscopy images were acquired with a 10x objective on an ArrayScanII station (Cellomics) and analyzed using a specialized image analysis algorithm (NuclearTranslocationV3 BioApplication, Cellomics). Nuclei were defined using the Hoechst dye signal obtained in channel 1, while the green fluorescent protein signal present in the nuclear mask, as well as a cytoplasmic ring was acquired in channel 2. The difference in GFP fluorescence intensity in the nuclear circle compared to the cytoplasmic ring was calculated for each cell and averaged over the acquired cell population (MEAN_CircRingAvgIntenDiffCh2). Determination of half-maximal inhibitory concentrations (IC_{50} values) was based on MEAN_CircRingAvgIntenDiffCh2 raw values. To evaluate relative STAT5 nuclear translocation in the assay, the mean of MEAN_CircRingAvgIntenDiffCh2 values (in octuplicates) from vehicle-treated cells without Epo (corresponding to blank value) was subtracted from the mean value with Epo stimulation. The resulting value was set to 100% STAT5 nuclear translocation. IC_{50} values were calculated using Excel Fit software (XLfit 4 curve fitting software for Microsoft Excel, ID Business Solutions Ltd).

Inhibitor profiling in Ba/F3 cell-based proliferation assays

Murine Ba/F3 cells are interleukin-3 (IL-3) dependent for growth and survival, but can be rendered to proliferate in an IL-3 independent manner by means of stably introducing oncogenic kinases (Warmuth et al., 2007). Ba/F3 cell lines dependent on different oncogenic kinases that are amenable to and available for inhibitor selectivity profiling at the Novartis Institutes for Biomedical Research and at the Genomics Institute of the Novartis Research Foundation have been described previously (Boulay et al., 2008; Melnick et al., 2006). CHZ868 (and where

indicated BBT594) was tested in Ba/F3 EpoR JAK2 V617F, Ba/F3 TEL-JAK2, Ba/F3 TEL-KDR(VEGFR2), Ba/F3 TEL-FLT3, Ba/F3 TEL-RET, Ba/F3 BCR-ABL, Ba/F3 BRAF V600E, Ba/F3 TEL-KIT, Ba/F3 TEL-PDGFRA, Ba/F3 TEL-PDGFRB, Ba/F3 TEL-ROS and Ba/F3 TEL-VEGFR1 cell proliferation assays over 48 hr as previously described (Adrian et al., 2006).

FISH on xenograft cells

Cells were isolated from viably frozen xenograft splenocytes or bone marrow. A direct preparation (DP) was made for FISH by treating the cells with hypotonic (0.075 M) potassium chloride) at 37°C for 20 min and then fixing them in 3:1 methanol:acetic acid. DPs were stored at -20°C until use for fluorescent in situ hybridization (FISH). *IGH@-CRLF2* rearrangements were detected using two commercially available probes: a dual color orange/green IGH@ breakapart probe (Abbott Molecular) with a blue probe for CRLF2 (Empire Genomics). Any *IGH@-CRLF2* rearrangement would separate the IGH probe's orange (3' flanking) and green (IGHV) signals and co-localize the split signal with the blue CRLF2 signal. Each probe was diluted in hybridization buffer according to manufacturer's instructions, then combined in a 1:2 ratio IGH@:CRLF2 to accommodate the weaker blue signal. FISH probes were mixed, applied to air-dried slides made from the xenograft DPs, sealed under glass coverslips, and denatured for 2 min at 72°C. After hybridization overnight at 37°C, slides were washed for 2 min at 72°C in 0.4X SSC/0.3%NP-40, 2 min at room temperature in 2X SSC/0.1% NP-40, air-dried, and mounted in antifade solution with DAPI counterstain (Vectashield, Vector Labs).

Hybridized slides were examined on an Olympus BX-51 microscope equipped with appropriate filters, and images captured with CytoVysion (Leica) imaging software. Scoring required image capture for most cells to determine co-localization of orange/green signals (IGH@) with blue

signals (CRLF2). When possible, 100 nuclei were scored for each specimen. A positive control cell line (MHH-CALL4) was similarly hybridized to confirm co-localization of CRLF2 with the IGH@ signal. Normal control cells (normal lymphoblasts) were similarly hybridized to determine the rate of apparent co-localization due to spatial proximity of the IGH@ and CRLF2 sequences without translocation.

Characterization of PDXs

All exons of 207 genes were sequenced at the Center for Cancer Genome Discovery (CCGD) at the Dana-Farber Cancer Institute (HemoSeq version 2; HemoSeq_v2) using an Illumina sequencing platform, as previously described (Odejide et al., 2014). The genes in HemoSeq v2 include:

ABCA7	BRAF	CNOT3	FBXW7	IRF8	MYC	PIGA	RPL10	STAT3	U2AF1
ABL1	BTG1	CREBBP	FLT3	JAK1	MYCN	PIK3AP1	RPL5	STAT5A	U2AF2
ALMS1	BTG2	CRLF2	FOXO1	JAK2	MYD88	PIK3CA	RUNX1	STAT5B	UBR5
ALPK2	BTK	CRLF2	GATA1	JAK3	NF1	PIK3CD	SENP6	STAT6	ULK4
APC	CARD11	CSF1R	GATA2	KDM4C	NFKB2	PIK3R1	SETBP1	SUZ12	VPS13A
ARID1A	CBL	CSF3R	GATA3	KDM6A	NFKBIA	PIM1	SETD2	SYK	WT1
ARID1B	CCND1	CTCF	GNA11	KIT	NLRP5	PLCG2	SF1	TAL1	XPO1
ARID2	CCND2	CTSS	GNA13	KLHL6	NOTCH1	POT1	SF3A1	TBL1XR1	ZFHX3
ARID3A	CCND3	CXCR4	GNAQ	KRAS	NOTCH2	PRDM1	SF3B1	TCF3	ZRSR2
ASXL1	CD200	DDX3X	GNAS	LEF1	NOTCH3	PRDM16	SGK1	TCF4	
ATM	CD36	DIS3	GNB1	LMO2	NPM1	PRKDC	SH2B3	TET2	
ATRX	CD58	DNMT3A	GNB2	LUC7L2	NR3C1	PRPF8	SMARCA2	TLR2	
B2M	CD79A	EBF1	HCK	MALT1	NRAS	PTEN	SMARCA4	TNFAIP3	
BACH2	CD79B	EED	ID3	MDM2	NT5C2	PTPN11	SMARCB1	TNFRSF14	
BCL10	CDK4	EP300	IDH1	MDM4	P2RY8	RAD21	SMC1A	TNFSF9	
BCL11A	CDK6	EPHA6	IDH2	MEF2B	P2RY8	RAPGEF1	SMC3	TP53	
BCL11B	CDKN2A	EPHA7	IKZF1	MEF2C	PAX5	RB1	SOCS1	TP63	
BCL2	CDKN2B	ETS1	IKZF2	MKI67	PCLO	REL	SRSF2	TP73	
BCL6	CEBPA	ETV6	IKZF3	MLL	PDGFC	RELN	SRSF6	TRAF2	
BCL7A	CELSR2	EZH2	IL7R	MLL2	PDGFRA	RFTN1	SRSF8	TRAF3	
BCR	CHD2	FAS	IRAK1	MLL3	PDGFRB	RHOA	STAG2	TRAF6	
BLNK	CIITA	FBXO11	IRF4	MUM1	PHF6	RNF213	STAT1	TYK2	

PDX splenocytes or bone marrow cells were purified by enrichment for human CD19 using human CD19 Microbeads (Miltenyi Biotech). Germline comparison for all PDXs was obtained from blood or bone marrow of patients in remission. Mutation analysis for single nucleotide variants (SNVs) was performed using MuTect v1.1.4 (Cibulskis et al., 2013) and annotated by Oncotator (Ramos et al., 2015). To filter out variants found in homologous regions of the mouse genome, we sequenced a representative mouse sample of the same genetic background as the host mice using HemoSeq_v2. Both the PDX and mouse samples were analyzed in paired mode using a matched normal (for human samples) or CEPH human cell line DNA (for mouse sample) as the project normal. We used the SomaticIndelDetector tool that is part of the GATK for INDEL calling, as described previously (Abedalthagafi et al., 2014).

Mouse model of rhEpo-induced polycythemia

Pharmacokinetic / pharmacodynamic and efficacy studies in the mouse model of rhEpo-induced polycythemia were carried out essentially as reported (Baffert et al., 2010). All animal experiments were performed in strict adherence to Swiss laws for animal welfare and approved by the Swiss Cantonal Veterinary Office of Basel-Stadt. CHZ868 was formulated in 0.5% methylcellulose / 0.5% Tween-80 for once daily oral dosing at 10 or 30 mg/kg. Detection of STAT5 phosphorylation in spleen lysates by Meso Scale Discovery was performed as previously described (Kubovcakova et al., 2013).

Intracellular BH3 Profiling / Cytochrome c release

BH3 profiling was performed as previously described (Montero et al., 2015; Pan et al., 2014). Briefly, cells were pelleted at 500xg for 5 min and resuspended in 100 µl 2% BSA/HBSS with

human CD45 antibody (BD Horizon, BV421clone HI30) 1:50 dilution, and human CD19 antibody (BDPharmigen PECy7 clone SJ25C1) 1:50 dilution. After a 30 min incubation on ice, cells were washed with PBS, pelleted, and resuspended in DTEB buffer at a density of $1x10^6$ cells/mL. 25 µl of cell suspension was added to each well containing 25 µl of DTEB buffer with 20 µg/mL Digitonin and peptides at twice their final concentration. Cells were incubated at room temperature for 60 min before terminating the exposure with 50 µl of 4% formaldehyde in PBS for 15 min at room temperature. Formaldehyde was then neutralized with 50 µl of N2 Buffer (1.7 M Tris, 1.25M glycine, pH 9.1) for 15 min at room temperature. To stain for retained cytochrome C, anti-cytochrome C clone 6H2.B4 conjugated to Alexafluor 488 (BD Bioscience) was diluted 1:50 in 10X stain buffer (1% Saponin, 10% BSA, 20% FBS in PBS) and 20 µl of this antibody/stain mixture was added to each well for a final antibody dilution of 1:360. Cells were stained overnight at 4°C and flow cytometry data acquired using a BD FACSCanto II.

Lineage and progenitor cell staining and sorting

To investigate the effect of JAK2 inhibition on normal hematopoiesis, wild-type C57B6/J x FVB/NJ F1 hybrid mice were treated with either vehicle (n=8) or CHZ868 30 mg/kg/d (n=8) for 44 days. Peripheral blood was collected every week to perform Complete Blood Counts (CBCs) using a Hemavet 950 (Drew Scientific). Serum erythropoietin levels were measured with the Mouse Erythropoietin Quantikine ELISA Kit (R&D Systems).

4 mice from each group were sacrificed after 44 days of treatment to compare hematopoietic cell populations in bone marrow. For lineage-positive cells, bone marrow cells were blocked with normal rat IgG (10 µg/10^6 cells, R&D Systems) and stained with antibodies against Gr-1 (RB6-8C5), CD11b (M1/70), CD3 (17A-2), TER119, B220 (RA3-6B2), CD45 (30-F11), or Isotype

control (RTK4530). All antibodies were PB-conjugated and purchased from BioLegend. Stained cells were analyzed using a FACSCanto II (Becton Dickinson) in the DFCI Hematologic Neoplasia FACS Core.

For lineage-negative cells, bone marrow cells were stained with the lineage cocktail antibodies: B220 (RA3-6B2), CD3 (17A2), Mac-1 (M1/70), Gr-1 (RB6-8C5), TER119, CD4 (RM4-5), CD8 (53-6.7), Il7R (A7R34), IgM (R6-60.2), and CD19 (1D3). Lin^+ cells were partially depleted using Sheep anti-rat IgG conjugated magnetic beads (Dynabeads, Life Technologies), and the remaining cells were stained with PE-Cy5.5 conjugated anti-rat IgG (Southern Biotech). Stained cells were then blocked with normal rat IgG. For the detection of myeloid progenitor populations, cells were stained with APC-Cy7-FcgRII/III (2.4G2), FITC-CD34 (RAM34), APC-c-Kit (2B8), and PE-Sca-1 (E13-161.7). For the detection of multipotent progenitor populations, cells were stained with FITC-CD34 (RAM34), PB-CD150 (TC1512F1), PE-Cy7-CD48 (HM48.1), APC-c-Kit (2B8), and PE-Sca-1 (E13-161.7). All antibodies except Il7R Ab (eBioscience) were purchased from BD Biosciences. Samples were collected 24 hr after the last dose of CHZ868 and analyzed on a Fortessa X-20 (Becton Dickinson) in the DFCI Hematologic Neoplasia FACS Core.

Transcriptional profiling analysis

The raw '.cel' files were converted into probeset-specific expression values using the Robust Multi-Array Average (RMA) summarization method (Irizarry et al., 2003) and current (version 18) Brainarray custom chip definition files based on Ensemble IDs (hta20hsensgcdf_18.0.0.cdf) (Dai et al., 2005) as implemented in the BioConductor package 'affy' (Gentleman et al., 2004). Ensemble IDs were converted to HUGO gene symbols using the 'biomaRt' package and

collapsed using the median. All data was log2 transformed. Cell line and PDX data were profiled separately and therefore treated as different batches.

Marker Selection, GSEA and Visualization

Differentially expressed genes following CHZ868 treatment were identified using the comparative marker selection module as embedded in GenePattern (Broad Institute, (Reich et al., 2006). GSEA of functionally validated E2F1 and MYC gene sets was performed as previously described (Chapuy et al., 2013; Subramanian et al., 2005). The tested apoptosis gene sets were obtained from the MSigDB repository (Broad Institute, Subramanian et al., 2005). The 100 most downregulated genes were visualized using GENE-E (http://www.broadinstitute.org/cancer/software/GENE-E/index.html).

Supplemental References

Abedalthagafi, M. S., Merrill, P. H., Bi, W. L., Jones, R. T., Listewnik, M. L., Ramkissoon, S. H., Thorner, A. R., Dunn, I. F., Beroukhim, R., Alexander, B. M.*, et al.* (2014). Angiomatous meningiomas have a distinct genetic profile with multiple chromosomal polysomies including polysomy of chromosome 5. Oncotarget *5*, 10596-10606.

Adrian, F. J., Ding, Q., Sim, T., Velentza, A., Sloan, C., Liu, Y., Zhang, G., Hur, W., Ding, S., Manley, P.*, et al.* (2006). Allosteric inhibitors of Bcr-abl-dependent cell proliferation. Nat Chem Biol *2*, 95-102.

Boulay, A., Breuleux, M., Stephan, C., Fux, C., Brisken, C., Fiche, M., Wartmann, M., Stumm, M., Lane, H. A., and Hynes, N. E. (2008). The Ret receptor tyrosine kinase pathway functionally interacts with the ERalpha pathway in breast cancer. Cancer research *68*, 3743-3751.

Chapuy, B., McKeown, M. R., Lin, C. Y., Monti, S., Roemer, M. G., Qi, J., Rahl, P. B., Sun, H. H., Yeda, K. T., Doench, J. G.*, et al.* (2013). Discovery and characterization of super-enhancer-associated dependencies in diffuse large B cell lymphoma. Cancer Cell *24*, 777-790.

Cibulskis, K., Lawrence, M. S., Carter, S. L., Sivachenko, A., Jaffe, D., Sougnez, C., Gabriel, S., Meyerson, M., Lander, E. S., and Getz, G. (2013). Sensitive detection of somatic point mutations in impure and heterogeneous cancer samples. Nat Biotechnol *31*, 213-219.

Dai, M., Wang, P., Boyd, A. D., Kostov, G., Athey, B., Jones, E. G., Bunney, W. E., Myers, R. M., Speed, T. P., Akil, H.*, et al.* (2005). Evolving gene/transcript definitions significantly alter the interpretation of GeneChip data. Nucleic Acids Res *33*, e175.

Gentleman, R., Carey, V., Bates, D., Bolstad, B., Dettling, M., Dudoit, S., Ellis, B., Gautier, L., Ge, Y., Gentry, J.*, et al.* (2004). Bioconductor: open software development for computational biology and bioinformatics. Genome Biol *5*, R80.

Irizarry, R. A., Bolstad, B. M., Collin, F., Cope, L. M., Hobbs, B., and Speed, T. P. (2003). Summaries of Affymetrix GeneChip probe level data. Nucleic Acids Res *31*, e15.

Karaman, M. W., Herrgard, S., Treiber, D. K., Gallant, P., Atteridge, C. E., Campbell, B. T., Chan, K. W., Ciceri, P., Davis, M. I., Edeen, P. T.*, et al.* (2008). A quantitative analysis of kinase inhibitor selectivity. Nat Biotechnol *26*, 127-132.

Kiel, M. J., Yilmaz, O. H., Iwashita, T., Yilmaz, O. H., Terhorst, C., and Morrison, S. J. (2005). SLAM family receptors distinguish hematopoietic stem and progenitor cells and reveal endothelial niches for stem cells. Cell *121*, 1109-1121.

Kubovcakova, L., Lundberg, P., Grisouard, J., Hao-Shen, H., Romanet, V., Andraos, R., Murakami, M., Dirnhofer, S., Wagner, K. U., Radimerski, T., and Skoda, R. C. (2013). Differential effects of hydroxyurea and INC424 on mutant allele burden and myeloproliferative phenotype in a JAK2-V617F polycythemia vera mouse model. Blood *121*, 1188-1199.

Melnick, J. S., Janes, J., Kim, S., Chang, J. Y., Sipes, D. G., Gunderson, D., Jarnes, L., Matzen, J. T., Garcia, M. E., Hood, T. L.*, et al.* (2006). An efficient rapid system for profiling the cellular activities of molecular libraries. Proceedings of the National Academy of Sciences of the United States of America *103*, 3153-3158.

Odejide, O., Weigert, O., Lane, A. A., Toscano, D., Lunning, M. A., Kopp, N., Kim, S., van Bodegom, D., Bolla, S., Schatz, J. H.*, et al.* (2014). A targeted mutational landscape of angioimmunoblastic T-cell lymphoma. Blood *123*, 1293-1296.

Ramos, A. H., Lichtenstein, L., Gupta, M., Lawrence, M. S., Pugh, T. J., Saksena, G., Meyerson, M., and Getz, G. (2015). Oncotator: cancer variant annotation tool. Hum Mutat *36*, E2423-2429.

Reich, M., Liefeld, T., Gould, J., Lerner, J., Tamayo, P., and Mesirov, J. P. (2006). GenePattern 2.0. Nat Genet *38*, 500-501.

Subramanian, A., Tamayo, P., Mootha, V. K., Mukherjee, S., Ebert, B. L., Gillette, M. A., Paulovich, A., Pomeroy, S. L., Golub, T. R., Lander, E. S., and Mesirov, J. P. (2005). Gene set enrichment analysis: a knowledge-based approach for interpreting genome-wide expression

profiles. Proceedings of the National Academy of Sciences of the United States of America *102*, 15545-15550.

Warmuth, M., Kim, S., Gu, X. J., Xia, G., and Adrian, F. (2007). Ba/F3 cells and their use in kinase drug discovery. Curr Opin Oncol *19*, 55-60.